



OPEN

Convolutional neural network algorithm trained on lumbar spine radiographs to predict outcomes of transforaminal epidural steroid injection for lumbosacral radicular pain from spinal stenosis

Jeoung Kun Kim¹ & Min Cheol Chang²✉

Little is known about the therapeutic outcomes of transforaminal epidural steroid injection (TFESI) in patients with lumbosacral radicular pain due to lumbar spinal stenosis (LSS). Using lumbar spine radiographs as input data, we trained a convolutional neural network (CNN) to predict therapeutic outcomes after lumbar TFESI in patients with lumbosacral radicular pain caused by LSS. We retrospectively recruited 193 patients for this study. The lumbar spine radiographs included anteroposterior, lateral, and bilateral (left and right) oblique views. We cut each lumbar spine radiograph image into a square shape that included the vertebra corresponding to the level at which the TFESI was performed and the vertebrae juxta below and above that level. Output data were divided into “favorable outcome” ($\geq 50\%$ reduction in the numeric rating scale [NRS] score at 2 months post-TFESI) and “poor outcome” ($< 50\%$ reduction in the NRS score at 2 months post-TFESI). Using these input and output data, we developed a CNN model for predicting TFESI outcomes. The area under the curve of our model was 0.920. Its accuracy was 87.2%. Our CNN model has an excellent capacity for predicting therapeutic outcomes after lumbar TFESI in patients with lumbosacral radicular pain induced by LSS.

Keywords Deep learning, Convolutional neural network, Lumbar spine, Spinal stenosis, Transforaminal epidural steroid injection

Lumbar spinal stenosis (LSS) is caused by narrowing of the lumbar spinal canal or lumbar vertebral foramen¹. LSS typically results from degenerative changes in the spine, including degeneration of the disc, formation of osteophytes, and thickening of spinal ligaments¹. These degenerative changes cause the narrowing of space that is available for the neural and vascular elements in the lumbar spine². LSS can cause pressure on the nerve roots and vascular structures². In addition to the compression of neurovascular structures in the lumbar spine, LSS causes an inflammatory response in which various inflammation-mediated cells and proinflammatory cytokines are involved, resulting in lumbosacral radicular pain³. The radicular pain from LSS may be aggravated, particularly during walking or standing for long periods⁴.

Conservative treatments such as oral medication, physical therapy, and injection procedures are used to control the lumbosacral radicular pain caused by LSS^{5,6}. Moreover, transforaminal epidural steroid injection (TFESI) is one of the most effective treatments for alleviating pain from LSS^{3,6}. Corticosteroids inhibit the synthesis of various proinflammatory mediators⁷.

The prediction of therapeutic outcomes after TFESI is important because it allows clinicians to elucidate a therapeutic plan for lumbosacral radicular pain due to LSS. Previous studies have evaluated outcomes according to stenosis severity observed on magnetic resonance imaging (MRI)^{3,8}. However, the prognostic evaluation

¹Department of Business Administration, School of Business, Yeungnam University, Gyeongsan-si, Republic of Korea. ²Department of Physical Medicine and Rehabilitation, College of Medicine, Yeungnam University, 317-1, Daemyungdong, Namku, Daegu 705-717, Republic of Korea. ✉email: wheel633@gmail.com

methods of the previous studies only showed a tendency of the therapeutic outcomes and did not provide individualized outcomes based on the specific structural characteristics of each patient^{3,8}. Furthermore, MRI is expensive and not easily accessible. We believe it is possible to assume the degree of spinal stenosis by assessing degenerative findings in lumbar spine radiographs, such as disc space narrowing, osteophyte formation, and facet degeneration⁹. Lumbar spine radiographs can be easily performed because almost all clinics and hospitals are equipped with a radiographic imaging machine, and the cost for patients is relatively low. However, at present, no study has analyzed the therapeutic outcomes of TFESI based on findings visible in lumbar spine radiographs.

Machine learning (ML) is a computer algorithm that can automatically learn from data without the need for explicit programming^{10–12}. ML is known for its ability to overcome the limitations of existing image analysis techniques and enable breakthroughs in the field of image analysis^{10–12}. Deep learning (DL) is an advanced ML approach that uses many hidden layers to build artificial neural networks with structures and functions similar to those of the human brain. It can learn from unstructured and perceptual image data, and several studies have demonstrated that the DL technique can outperform traditional ML techniques^{13–15}. A convolutional neural network (CNN) is a representative DL model specializing in image analysis^{16,17}. We believe that the CNN model can recognize and analyze the findings related to spinal degeneration on lumbar spine radiographs and could help predict the therapeutic outcome of TFESI. Furthermore, CNN can enable personalized prediction of therapeutic outcomes based on each patient's images.

In the current study, we used lumbar spine radiographs as input data and trained a CNN model to predict therapeutic outcomes after lumbar TFESI in patients with lumbosacral radicular pain caused by LSS.

Results

Table 1 summarizes the sample characteristics of the proposed model and its performance measures. This study utilized 193 samples, with a training set comprising 79.8% (154 samples) and a validation set comprising 20.2% (39 samples). The training set had a 'favorable outcome' to 'poor outcome' ratio of 38.3–61.7%, while the validation set had a ratio of 33.3–66.7%. The trained model demonstrated robust performance with a training accuracy of 94.2% and an AUC of 0.983 (95% CI [0.967–1.000]). The validation accuracy was also high at 87.2%, with an AUC of 0.920 (95% CI [0.834–1.000]) (Fig. 1).

In terms of class-specific performance, for the 'favorable outcome' set, the precision was 0.733, recall was 0.917, and F1-score was 0.815. For the 'poor outcome set' the model showed a precision of 0.958, recall of 0.852, and F1-score of 0.902. The macro average across classes was a precision of 0.846, recall of 0.884, and F1-score of 0.858, while the weighted average was a precision of 0.889, recall of 0.872, and F1-score of 0.875.

These results suggest that the model is highly accurate and distinguishes between the 'favorable outcome' and 'poor outcome' with a particularly strong performance in identifying the 'favorable outcome'. However, there is scope for improvement in the precision for the 'favorable outcome'.

Figure 2 provides additional information on the model's characteristics through confusion matrix analysis for the validation data. The confusion matrix shows that the model correctly predicted 11 out of 12 patients who showed 'favorable outcomes' (91.7% precision). Also, the model correctly predicted 23 out of 27 patients with 'poor outcomes' (85.2% recall).

Discussion

In our study, we developed a CNN algorithm for predicting therapeutic outcomes of lumbar TFESI in patients with lumbosacral radicular pain following LSS. The accuracy of our algorithm was 87.2%, and the AUC was 0.920. Considering that AUCs of 0.7–0.8, 0.8–0.9, and > 0.9 are considered as having acceptable, excellent, and

Developed model					
Sample size	154, 79.8% for training, 39, 20.2% for validation, total 193				
Sample ratio	Favor outcome: 59, 38.3%; Poor outcome: 95, 61.7% for training, total 154 Favor outcome: 12, 33.3%; Poor outcome: 27, 66.7% for validation, total 39				
Model details	- EfficientNetV2S CNN model with full training				
	- SGD optimizer, ReLU activation				
	- Learning rate 3e-05, batch size 16				
	- Batch normalization and dropout for regularization				
	- ROI image resized to (384 × 384)				
	- Specificity: 96.8% for training and 85.2% for validation				
	- Training accuracy: 94.2%, AUC 0.983 with 95% CI [0.967–1.000]				
	- Validation accuracy: 87.2%, AUC 0.920 with 95% CI [0.834–1.000]				
Model performance (validation data)	Class	Precision	Recall (sensitivity)	F1-score	Support
	Favor outcome (1)	0.733	0.917	0.815	12
	Poor outcome (0)	0.958	0.852	0.902	27
	Macro average	0.846	0.884	0.858	39
	Weighted average	0.889	0.872	0.875	39

Table 1. Model performance analysis. CNN, convolutional neural network; SGD, stochastic gradient descent; ReLU, rectified linear units; ROI, region of interest; AUC, area under the curve; CI, confidence interval.

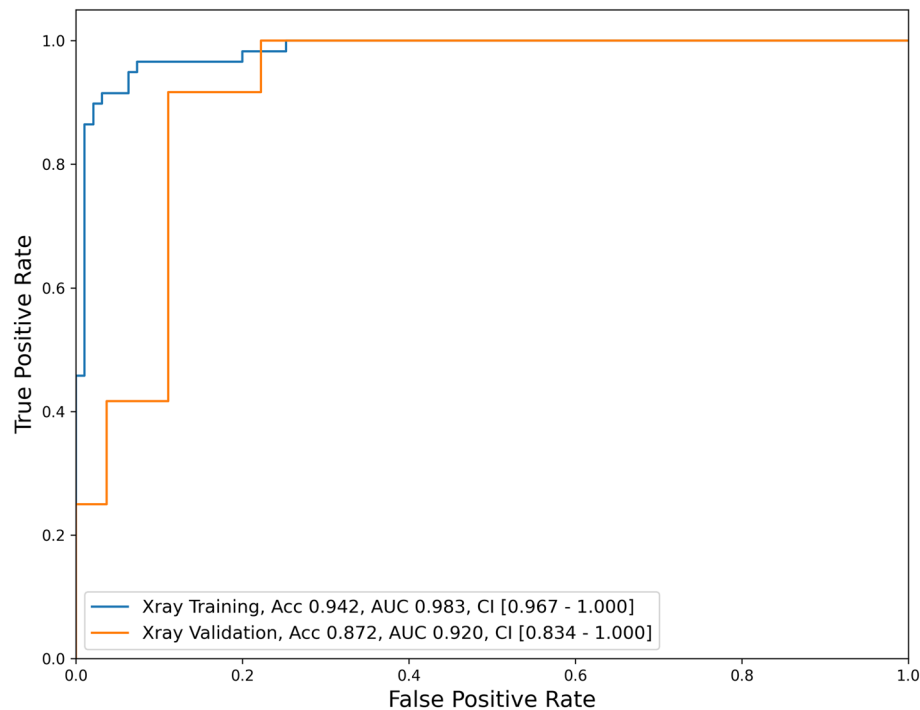


Figure 1. Receiver operating characteristic curves for the validation and test datasets of our developed model. Acc, accuracy; AUC, area under the curve; CI, confidence interval.

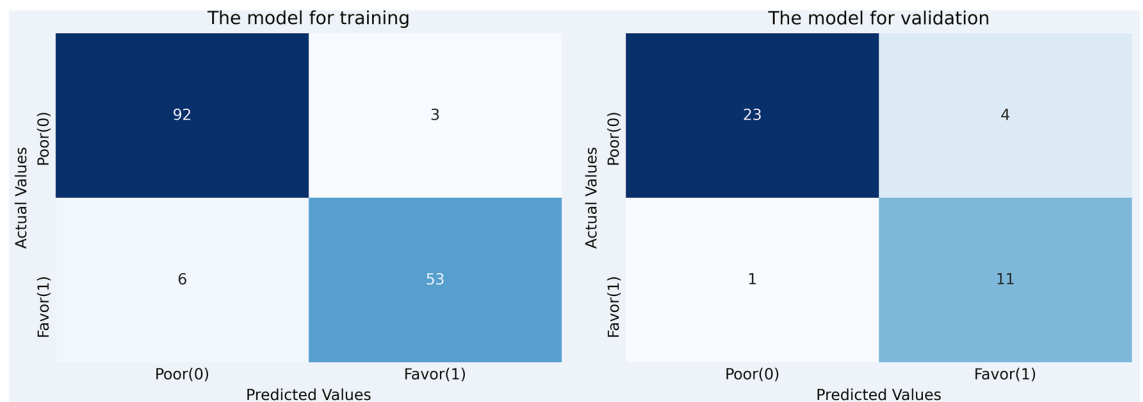


Figure 2. The confusion matrix for our developed model.

outstanding diagnostic capacities, respectively, the ability of our CNN model that was developed using lumbar radiographs as input data seems to be excellent¹⁸.

While neural networks and other various algorithms have been utilized for the past 50 years, developments in the field of CNNs constitute significant accomplishments^{14,17}. The multiple convolutional and pooling layers of the CNN algorithm enable the identification of radiologic features or other image-based data and assign weights to important features^{16,17}. Also, the CNN algorithm is less affected by distortions, horizontal or vertical shifts, contrasts, angles, and partial masks in images; it also requires less computer memory, which allows for more effective algorithm training¹⁹. In accordance with these advantages of the CNN algorithm, our algorithm is expected to accurately identify key features influencing the therapeutic prognosis after TFESI in lumbar radiographs of patients with LSS.

Previous studies have evaluated therapeutic outcomes after TFESI in patients with LSS for alleviating lumbosacral radicular pain^{3,8}. In 2018, Chang et al. evaluated the outcome of TFESI according to the severity of lumbar foraminal spinal stenosis (LFSS)³. Of 31 patients with mild to moderate LFSS, 27 patients (87.1%) showed favorable outcomes ($\geq 50\%$ pain reduction of initial pain at 3 months post-treatment). Of 26 patients with severe LFSS, 11 (42.5%) reported successful pain relief. In 2020, Do et al. evaluated the therapeutic outcomes of interlaminar epidural steroid injection in patients with chronic radicular pain according to the degree of lumbar central spinal stenosis (LCSS)⁸. At 3 months after TFESI, nine (30.0%) of 30 patients with moderate LCSS showed

favorable outcomes ($\geq 50\%$ pain reduction of initial pain at 3 months post-treatment). Five (17.9%) of 28 patients with severe LCSS reported successful pain relief. However, these research results described only overall trends in therapeutic outcomes based on radiologic findings, such that it remains difficult to discern the favorable and poor therapeutic outcomes of an individual patient. In contrast, our algorithm can determine an individual's therapeutic outcomes when inputting each patient's lumbar radiographs into the algorithm.

Regarding studies that developed a DL algorithm to predict therapeutic outcomes after TFESI, to the best of our knowledge, two studies have been published^{20,21}. In 2022, Kim et al. collected whole T2-weighted sagittal lumbar spine MR images from 503 patients with chronic lumbosacral radicular pain²⁰. Similar to our study, the favorable and poor outcomes were defined as $\geq 50\%$ and $< 50\%$ reduction at 2-month follow-up after TFESI, respectively. Kim et al. reported that the accuracy for predicting the therapeutic outcome of TFESI was 76.2%, and the AUC was 0.827. In 2023, Wang et al. recruited 288 patients with radicular pain due to cervical foraminal stenosis²¹. The authors collected single T2-axial spine MR images for each patient. They also defined $\geq 50\%$ and $< 50\%$ reduction at 2-month follow-up after TFESI as favorable and poor outcomes, respectively. The accuracy of the developed model for predicting the outcome after TFESI was 79.3%, and the AUC was 0.801. Therefore, our study is the first to demonstrate the usefulness of a DL model trained using radiographs in predicting the therapeutic outcomes of spinal injections for radicular pain.

Integrating our research results with a cloud system could significantly enhance its accessibility and scalability. A cloud-based platform would allow for deployment of the developed model across healthcare settings, enabling real-time analysis of lumbar spine radiographs. This approach would facilitate a centralized database for training and updating the model with new data, improving its accuracy over time. Moreover, cloud integration supports collaborative efforts among healthcare professionals and researchers, allowing for seamless sharing of insights and advancements in the treatment of lumbosacral radicular pain caused by LSS. By leveraging cloud technology, the research outcomes can be made more widely available, offering optimized treatment plans on a global scale.

In conclusion, we found that a CNN model trained using four radiographs (the anteroposterior, lateral, and left and right obliques) per each patient had an excellent capacity (accuracy = 87.2%, AUC = 0.920) for predicting the therapeutic outcomes after lumbar TFESI in patients with lumbosacral radicular pain due to LSS. We believe that our developed model could be effectively applied as a supplementary tool in clinical practice by pain physicians. Our study had several limitations. (1) A relatively small number of patients were included. (2) We collected images from a single hospital. To increase the generalizability of our results, lumbar radiographs collected from multiple hospitals should be used as input data for the CNN training algorithm. (3) We assumed that the patients' pain was caused solely by single-level LSS. However, in reality, it is possible that the pain was associated with multiple levels of LSS. Therefore, for more accurate analysis, it is preferable to use the entire lumbar spine image as input data for developing the DL algorithm. (4) We used only the NRS as output data. If functional data were used instead, the developed algorithm could provide more information. (5) For developing the DL algorithm, we used only lumbar spine radiographs as input data. Incorporating MRI data along with lumbar spine radiographs as input data could further improve the prediction accuracy of therapeutic outcomes after lumbar TFESI.

Materials and methods

Participants

This retrospective observational study involved 193 patients (mean age = 74.3 ± 9.8 years, men: women = 71:122, injection levels L3:L4:L5:S1 = 2:3:24:156:8, right: left: bilateral = 69:68:56) who visited the spine center of a university hospital and underwent lumbar TFESI for LSS between January 2013 and December 2021. The inclusion criteria for this study were as follows: (1) single-level lumbar TFESI for segmental pain that radiated to the lower extremity due to LSS; (2) ≥ 3 months history of a symptomatic lumbosacral radicular pain with > 3 on a numerical rating scale (NRS-11; 0 = no pain; 10 = the worst pain) prior to TFESI; (3) $\geq 50\%$ temporary pain relief following a diagnostic nerve block with 1 mL of 2% lidocaine; and (4) MRI and electrophysiological findings corresponding to the clinical manifestations. The data of patients with a history of spinal surgery, such as lumbar fusion or laminectomy, before TFESI were excluded. The study protocol was approved by the institutional review board of Yeungnam university hospital, which waived the requirement for written informed consent owing to the retrospective nature of this study. The study was conducted in accordance with the Declaration of Helsinki.

TFESI procedures

TFESI was conducted using the standard method described in a previous study. All injections were performed by a single interventional physiatrist specializing in spinal injections. A strict aseptic technique was used to perform the TFESI procedures. Patients were prone, and C-arm fluoroscopy (Siemens, Erlangen, Germany) was used to aid level identification and needle placement. Lidocaine 1% was administered at the needle insertion site, and the tip of a 25-gauge 90-mm spinal needle with a bend at the tip to allow for guidance was positioned between the lateral vertebral body and the 6 o'clock position below the pedicle. Lateral fluoroscopic imaging demonstrated the presence of the needle tip between the spinal lamina margin and the posterior vertebral body. Under anteroposterior fluoroscopy, 0.3 mL of non-ionic contrast material was injected to confirm the absence of vascular uptake and spread of contrast into the foramen. Subsequently, another injection of the contrast medium was performed under real-time fluoroscopic monitoring, and 20 mg (0.5 mL) of triamcinolone with 0.5 mL of bupivacaine hydrochloride and 1 mL of normal saline was injected.

Images used for the DL algorithm (input data)

Lumbar spine radiographs were used as input data for developing the DL algorithm. Lumbar spine radiographs that were used as input data include the anteroposterior, lateral, and bilateral oblique (left and right oblique)

Layer (type)	Output Shape	Param #
anteroposterior img (InputLayer)	[(None, 384, 384, 3)]	0
lateral img (InputLayer)	[(None, 384, 384, 3)]	0
left oblique img (InputLayer)	[(None, 384, 384, 3)]	0
right oblique img (InputLayer)	[(None, 384, 384, 3)]	0
efficientnetv2-s (Functional)	(None, None, None, 1280)	2,033,136
global_average_pooling2d (GlobalAveragePooling2D)	(None, 1280)	0
global_average_pooling2d_1 (GlobalAveragePooling2D)	(None, 1280)	0
global_average_pooling2d_2 (GlobalAveragePooling2D)	(None, 1280)	0
global_average_pooling2d_3 (GlobalAveragePooling2D)	(None, 1280)	0
concatenate (Concatenate)	(None, 5120)	0
dense (Dense)	(None, 1024)	5,243,904
batch_normalization (BatchNormalization)	(None, 1024)	4,096
Dropout (Dropout)	(None, 1024)	0
Dense_1 (Dense)	(None, 1024)	1,049,600
batch_normalization_1 (BatchNormalization)	(None, 1024)	4,096
dense_2 (Dense)	(None, 1)	1,025
Total params: 26,634,081 (101.60 MB) Trainable params: 26,476,113 (101.00 MB) Non-trainable params: 157,968 (617.06 KB)		

Table 2. TFESI model detail.

views. Oblique lumbar radiographs were obtained from a 45° anteroposterior orientation on both the left and right sides of each patient. Additionally, we cut each lumbar spine radiograph image into a square shape that included the vertebra corresponding to the level at which the TFESI was performed, as well as the vertebrae juxta below and above that level.

To prepare data for DL, the region of interest (ROI) was isolated, with images segmented by a physiatrist to delineate regions with critical lesions, and image dimensions were standardized. This ROI protocol positively influenced the learning efficacy of the DL model. Furthermore, image features were normalized prior to their input into the CNN model to optimize generalization capability. This approach enhances applicability of the model across diverse datasets within the medical imaging domain. Medical imaging requires precise lesion detection, therefore attributes such as brightness adjustment, blurring, and noise were not utilized in image processing methodology in this study.

Measurement of therapeutic outcome (output data)

Pain severity at pretreatment and 2-month follow-up after TFESI was assessed on the NRS (0 = no pain; 10 = worst pain). The NRS data were collected via chart review. A “favorable outcome” was defined as a $\geq 50\%$ reduction in NRS score at 2 months post-TFESI versus the pretreatment NRS score. A “poor outcome” was defined as a $< 50\%$ reduction in NRS score at 2 months post-TFESI versus the pretreatment score. To validate the change in pain reduction, NRS scores were evaluated by assessing the difference between the pretreatment NRS scores and the 2-month post-treatment scores ($\text{change in NRS } [\%] = [\text{pretreatment score} - 2 \text{ months post-TFESI score}] / \text{pretreatment score} \times 100$).

DL algorithms

Python 3.8.10, scikit-learn 1.1.2, and TensorFlow 2.13.0 with Keras were used to develop the CNN model for predicting TFESI outcomes. We concurrently fed four X-ray ROI images (anteroposterior, lateral, left oblique, and right oblique) into the EfficientNetV2S CNN model for training. We employed a range of optimizers, learning rates, and batch sizes, integrating dropout regularization techniques to mitigate overfitting. Table 2 provides detailed information about the proposed model. The table is based on the outputs generated using TensorFlow’s model.summary() function. Figure 3 offers a concise summary of each phase within the model training procedure.

Statistical analysis

Statistical analyses were executed utilizing Python 3.8.10 and scikit-learn version 1.1.2. A receiver operating characteristic (ROC) curve analysis was conducted, and the area under the curve (AUC) was computed. The 95% confidence interval (CI) for the AUC was determined following the method outlined by DeLong et al.²². Scikit-learn was employed for computing both the ROC curve and AUC. The classification report function in scikit-learn was employed to compute the accuracy, class-specific precision, recall, and F1 score.

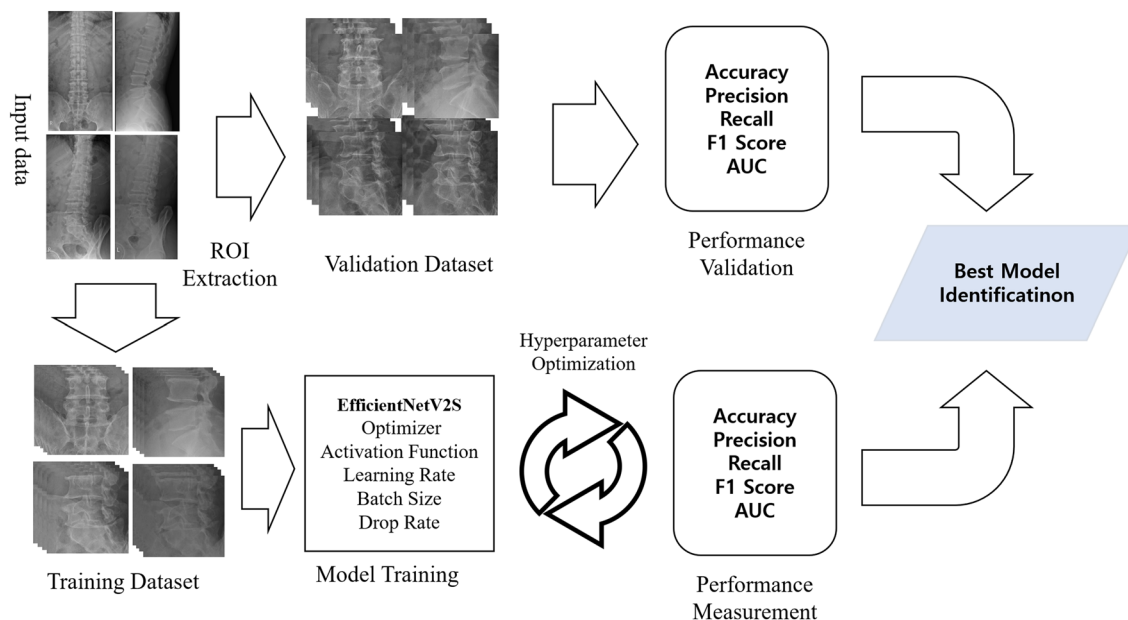


Figure 3. Diagram of the process for the development of the deep learning model for predicting the therapeutic outcome after transforaminal epidural steroid injection in patients with lumbosacral radicular pain due to lumbar spinal stenosis. ROI, region of interest; AUC, area under the curve.

Data availability

Some or all data, models, or code generated or used during the study are available from the corresponding author by request.

Received: 15 October 2023; Accepted: 9 April 2024

Published online: 11 April 2024

References

- Radu, A. S. & Menkès, C. J. Update on lumbar spinal stenosis. Retrospective study of 62 patients and review of the literature. *Rev. Rhum. Engl. Ed.* **65**, 337–345 (1998).
- Akuthota, V., Lento, P. & Sowa, G. Pathogenesis of lumbar spinal stenosis pain: Why does an asymptomatic stenotic patient flare?. *Phys. Med. Rehabil. Clin. N. Am.* **14**, 17–28 (2003).
- Chang, M. C. & Lee, D. G. Outcome of transforaminal epidural steroid injection according to the severity of lumbar foraminal spinal stenosis. *Pain. Physician.* **21**, 67–72 (2018).
- Malik, K. N., Giberson, C., Ballard, M., Camp, N. & Chan, J. Pain management interventions in lumbar spinal stenosis: A literature review. *Cureus.* **15**, e44116 (2023).
- Fornari, M. *et al.* Conservative treatment and percutaneous pain relief techniques in patients with lumbar spinal stenosis: WFNS Spine Committee Recommendations. *World. Neurosurg.* **X**, 7, 100079 (2020).
- Jang, S. H. & Chang, M. C. At least 5-year follow-up after transforaminal epidural steroid injection due to lumbar radicular pain caused by spinal stenosis. *Pain. Pract.* **20**, 748–751 (2020).
- Barnes, P. J. How corticosteroids control inflammation: Quintiles Prize Lecture 2005. *Br. J. Pharmacol.* **148**, 245–254 (2006).
- Do, K. H., Kim, T. H. & Chang, M. C. Effects of interlaminar epidural steroid injection in patients with moderate to severe lumbar central spinal stenosis: A prospective study. *Ann. Palliat. Med.* **9**, 163–168 (2020).
- Perera, R. S. *et al.* Associations between disc space narrowing, anterior osteophytes and disability in chronic mechanical low back pain: A cross sectional study. *BMC. Musculoskelet. Disord.* **18**, 193 (2017).
- Choo, Y. J. & Chang, M. C. Use of machine learning in the field of prosthetics and orthotics: A systematic narrative review. *Prosthet. Orthot. Int.* **47**, 226–240 (2023).
- Janiesch, C., Zschech, P. & Heinrich, K. Machine learning and deep learning. *Electron. Markets.* **31**, 685–695 (2021).
- Sarker, I. H. Machine learning: Algorithms, real-world applications and research directions. *SN. Comput. Sci.* **2**, 160 (2021).
- Alzubaidi, L. *et al.* Review of deep learning: Concepts, CNN architectures, challenges, applications, future directions. *J. Big. Data.* **8**, 53 (2021).
- Chang, M. C. *et al.* The use of artificial intelligence to predict the prognosis of patients undergoing central nervous system rehabilitation: A narrative review. *Healthcare.* **11**, 2687 (2023).
- Koutsoukas, A., Monaghan, K. J., Li, X. & Huan, J. Deep-learning: Investigating deep neural networks hyper-parameters and comparison of performance to shallow methods for modeling bioactivity data. *J. Cheminform.* **9**, 42 (2017).
- Kim, J. K., Choo, Y. J., Shin, H., Choi, G. S. & Chang, M. C. Prediction of ambulatory outcome in patients with corona radiata infarction using deep learning. *Sci. Rep.* **11**, 7989 (2021).
- Yamashita, R., Nishio, M., Do, R. K. G. & Togashi, K. Convolutional neural networks: An overview and application in radiology. *Insights. Imaging.* **9**, 611–629 (2018).
- Mandrekar, J. N. Receiver operating characteristic curve in diagnostic test assessment. *J. Thorac. Oncol.* **5**, 1315–1316 (2010).
- Kim, J. K. *et al.* Deep learning analysis to automatically detect the presence of penetration or aspiration in video fluoroscopic swallowing study. *J. Korean. Med. Sci.* **37**, e42 (2022).
- Kim, J. K., Wang, M. X. & Chang, M. C. Deep learning algorithm trained on lumbar magnetic resonance imaging to predict outcomes of transforaminal epidural steroid injection for chronic lumbosacral radicular pain. *Pain. Physician.* **25**, 587–592 (2022).

21. Wang, M. X., Kim, J. K. & Chang, M. C. Deep learning algorithm trained on cervical magnetic resonance imaging to predict outcomes of transforaminal epidural steroid injection for radicular pain from cervical foraminal stenosis. *J. Pain. Res.* **16**, 2587–2594 (2023).
22. DeLong, E. R., DeLong, D. M. & Clarke-Pearson, D. L. Comparing the areas under two or more correlated receiver operating characteristic curves: a nonparametric approach. *Biometrics.* **44**, 837–845 (1998).

Author contributions

J.K.K.: study design, data collection, data analysis, and manuscript writing/editing. M.C.C.: study design, data collection, data analysis, and manuscript writing/editing, and supervision.

Funding

This work was supported by the 2023 Yeungnam University Research Grant.

Competing interests

The authors declare no competing interests.

Additional information

Correspondence and requests for materials should be addressed to M.C.C.

Reprints and permissions information is available at www.nature.com/reprints.

Publisher's note Springer Nature remains neutral with regard to jurisdictional claims in published maps and institutional affiliations.



Open Access This article is licensed under a Creative Commons Attribution 4.0 International License, which permits use, sharing, adaptation, distribution and reproduction in any medium or format, as long as you give appropriate credit to the original author(s) and the source, provide a link to the Creative Commons licence, and indicate if changes were made. The images or other third party material in this article are included in the article's Creative Commons licence, unless indicated otherwise in a credit line to the material. If material is not included in the article's Creative Commons licence and your intended use is not permitted by statutory regulation or exceeds the permitted use, you will need to obtain permission directly from the copyright holder. To view a copy of this licence, visit <http://creativecommons.org/licenses/by/4.0/>.

© The Author(s) 2024